

Experimental Simulation of Melt Dispersion at Low Pressure in an Annular Cavity

Mireia Gargallo, Leonhard Meyer

Forschungszentrum Karlsruhe, Institut für Kern-und Energietechnik, Postfach 3640
76021 Karlsruhe, Germany, Email: mireia.gargallo@iket.fzk.de

ABSTRACT

Melt dispersion experiments at low system pressures were conducted in the DISCO-C test facility, where an annular cavity design is modeled in a scale 1:18. In these test series only cold simulant materials were used: nitrogen and helium instead of steam, and water and a bismuth alloy instead of melt. Failure pressures under 2 MPa, and different breach geometries and positions were studied. The experimental results have shown, that the failure mode of the lower head plays a predominant role in the dispersion process. It has also been observed, that even at low system pressures large amounts of melt can be carried out of the cavity in form of a liquid film that flows up at the cavity wall into the compartments as well as in form of dispersed droplets. In a series of three experiments, drop sizes as well as drop and liquid jet velocities were measured. Moreover, gas blow down velocities in the annular gap were measured in certain experiments.

INTRODUCTION

Up to now, melt dispersal and DCH phenomena have been investigated intensively mainly for cavity designs with large instrument tunnels leading into the compartments, relatively high melt ejection pressures and small holes centered at the lower head [1, 2, 3]. However, only few works have studied these phenomena with an annular cavity design similar to that of some European PWRs and the European Pressurized Reactor (EPR), where the only large pathway out of the cavity is the narrow annular gap between the reactor pressure vessel (RPV) and the cavity wall. Moreover, there are few works which study RPV failures during low pressure melt ejection scenarios. Therefore, the DISCO (Dispersion of Simulated Corium) program is aimed at low failure pressures, different failure modes and larger breach sizes using an annular cavity design similar to that of the planned EPR.

The experimental program has been divided into three parts:

-Two experiments at the Sandia National Laboratories (SNL) in cooperation with Forschungszentrum Karlsruhe (FZK), Institut de Protection et de Sûreté Nucléaire (IPSN) and the U.S. Nuclear Regulatory Commission (NRC) [4]. These tests were performed with thermite melt, steam and a prototypic atmosphere in the containment in a scale 1:10. The main results showed that even failures at low system pressures can lead to a considerable ejection of liquid out of the cavity.

-A series of experiments using cold simulant materials to study the fluid dynamics of the dispersion process in the test facility DISCO-C (EPR geometry, scale 1:18) at FZK. The fluids employed are water or a bismuth alloy ($\rho = 9230 \text{ kg m}^{-3}$, $T_{\text{melt}} = 60^\circ\text{C}$, similar to Wood's metal) instead of corium, and nitrogen or helium instead of steam. This part of the experimental program has been practically concluded. The results of these experiments are presented here, focusing especially on the results obtained in a series of experiments where drop and liquid jet velocities as well as drop sizes were measured. These parameters are predominant to characterize energy transfer processes between the dispersed corium and the containment atmosphere and can be used for validation of scaling models [5] and CFD-Codes [6].

-A third series of selected tests in the DISCO-H facility, also at FZK. With the same scale as DISCO-C, experiments will be carried out with thermite melt, steam and a prototypic atmosphere in the containment to study thermal and chemical effects in the dispersion process.

DESCRIPTION OF THE TEST FACILITY

Experimental set up

The experimental set up is shown in Fig. 1. The main components of the test facility are:

1. The pressure vessel (PV), with a total volume of 0.0879 m^3 , consists of a steel pipe that models the volume of the EPR pressure vessel and the volume of part of the RCS. A disk holding 8 pipes separates the two partial volumes in ratio 60:40 (RCS:RPV). The lower head of the RPV can hold $3.4 \cdot 10^{-3} \text{ m}^3$ of liquid, which corresponds to 20 m^3 or 160 t of corium.

2. The cavity, a Plexiglas cylinder with an inner diameter of 342 mm, is attached to the vessel support structure. The only flow path out of the cavity is the annular gap existing between the cavity itself and the RPV. This annular gap, with a total flow cross section of 0.02188 m^2 , leads to the main coolant lines and subsequently to the compartments. There is a second possible flow path out of the cavity through four ventilation openings in the lower part of the Plexiglas cylinder, which lead to the melt spreading room. However these openings were closed in all of the experiments except in an special one (S-01).

3. The eight main coolant lines are modeled each one by a rod inside a pipe. These nozzles have a total flow cross section of 0.03077 m^2 .

4. The compartments, eight boxes which model in volume the steam generator and pump rooms (0.3 m^3 and 0.131 m^3 each respectively), are connected to the nozzles and are placed on the vessel support structure around the RPV. They are covered by filters on their tops for the extraction of fog and drops. Two boxes have one Plexiglas wall to permit optical access for flow visualization.

5. A conical ring at the pressure vessel support, that represents a constriction for the flow, with 16 holes with a diameter of 26 mm. The total flow cross section through the vessel support reduces then to 0.01890 m^2 . There is a space behind this conical ring, where liquid can be collected during the experiments. To avoid this, the space was filled with silicon rubber up to the height of the 16 holes in some of the latter experiments.

Failure Modes

The DISCO-C experiments are the first which test the effect of different RPV failure geometries on the dispersal rates. The following failure modes of the lower head were studied:

1. Central breaches
2. Lateral holes
3. Lateral slots
4. Unzipping and tilting of the lower head

Central holes positioned at the bottom of the RPV were studied in the first series of experiments. The holes were closed by a rupture disk with an opening diameter somewhat larger than that of the hole. A similar construction was employed for lateral holes but they were placed 50 mm above the bottom of the lower head in a 45 degrees inclined axis. Lateral slots were also placed in a 45 degrees axis but with the lower edge 56.1 mm above the bottom of the calotte. With this configuration, a failure due to a side-peaked heat flux was modeled. Lastly, the complete rupture of the RPV bottom was modeled by unzipping and tilting of the lower head. To simulate such a failure, the lower head was supported by a vertical rod held by four bolts connected to detonators. By breaking the bolts, the rod was released and the lower head fell down attached at one side at the RPV. The flow cross section of the failure was defined by the height of four pedestals placed at the bottom of the cavity to stop the movement of the lower head. A scheme of all these failure modes is presented in Fig. 2.

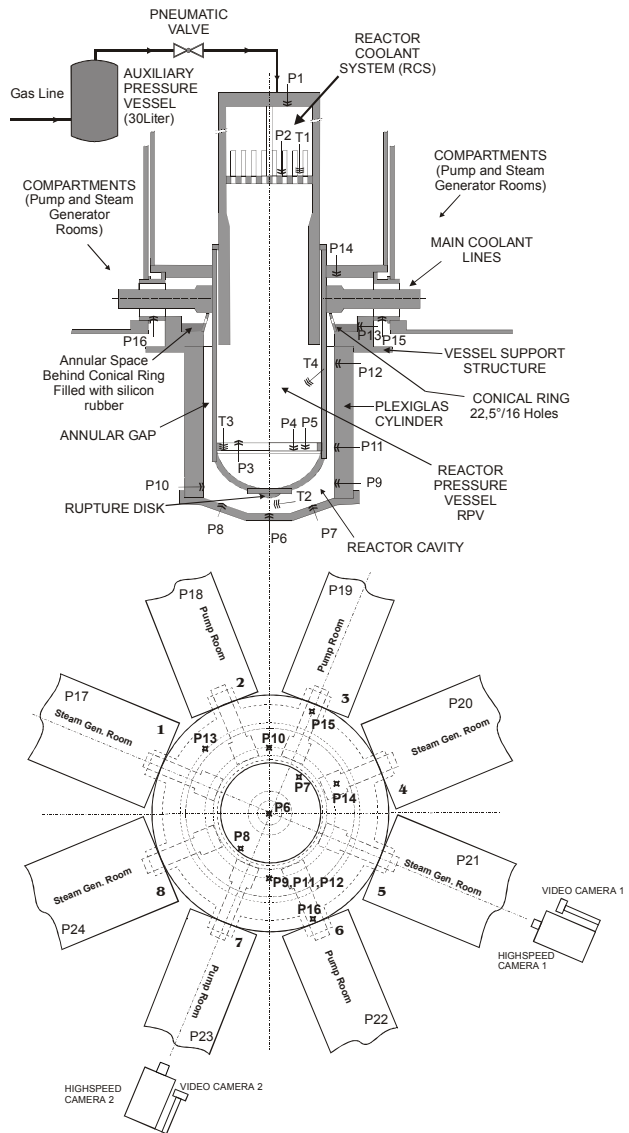


Fig. 1 The DISCO-C test facility

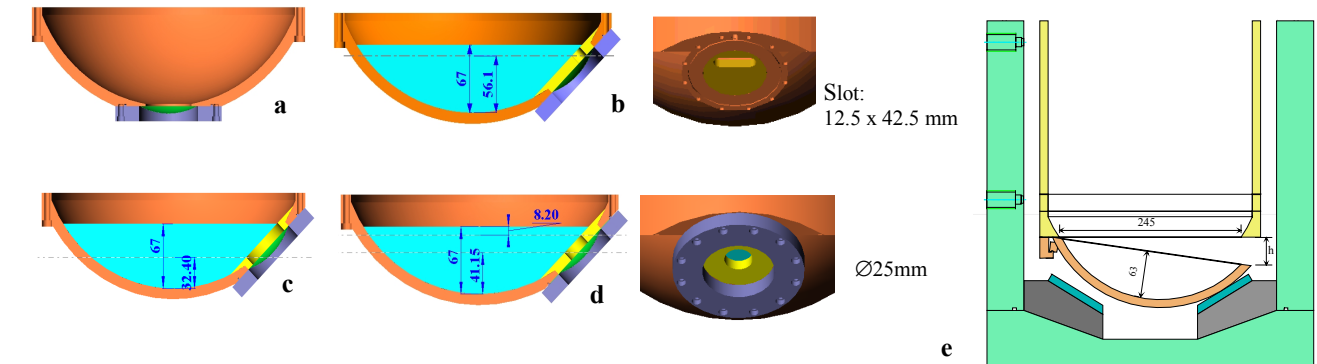


Fig. 2 Failure geometries used in DISCO-C

- a. Central hole
- b. Lateral slot, equivalent to $\text{Ø}25\text{mm}$
- c. Lateral hole, $\text{Ø}50 \text{ mm}$
- d. Lateral hole, $\text{Ø}25 \text{ mm}$

- e. Unzipping and tilting of the lower head

Geometry variations

To investigate the effect of different initial liquid pool depths a standpipe was mounted inside the pressure vessel in two experiments (Fig. 5). The standpipe can hold the same amount of liquid as the lower head. This geometry was also used by Bertodano et al. [7] and Kim et al. [8].

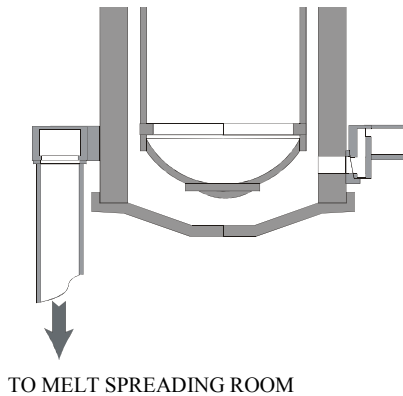


Fig. 3 Cavity with openings leading into the melt spreading room

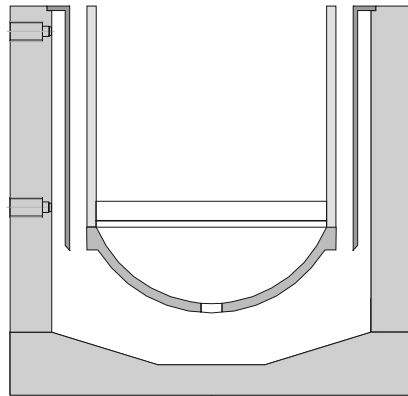


Fig. 4 Melt trapping device in the cavity

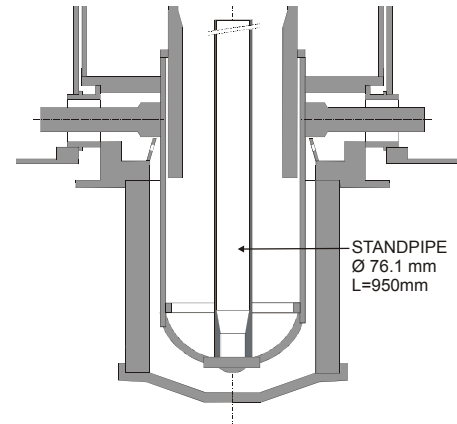


Fig. 5 Geometry for tests T-01 and T-02

Additionally, some tests with different cavity designs were performed. In one design, the diameter of the cavity was increased to make room for an extra cylinder, that should trap the liquid mass and prevent the dispersion out of the cavity (Fig. 4). The other modification in the cavity geometry deals with the venting openings of the reactor pit. There were four holes in the lower part of the pit that were connected by a circumferential channel and a tube to an extra compartment modeling the spreading room (Fig. 3).

EXPERIMENTAL PROCEDURE

The experiments were carried out in the following way:

The pressure vessel was filled at a pressure close to the failure pressure of the disk. Opening the pneumatic valve between the pressure vessel and an auxiliary vessel, filled at a higher pressure, the pressure in the pressure vessel was increased until the rupture disk broke. A break wire placed on the rupture disk gave the signal for the time mark $t = 0$ s and closed the pneumatic valve.

Pressure and temperature

Absolute pressures and temperatures were measured at the positions indicated in Fig. 1 during the transient with a sampling rate of 2.5 kHz. From these data blow down histories could be analyzed.

Dispersal Rates

The liquid fraction dispersed out of the cavity could be measured by weighing the compartments before and after each experiment (accuracy ± 0.1 g). The liquid that remained in the cavity was dried with a cloth and also weighed except for the case of metal alloy, because the liquid was already solid after the experiments and could be weighed directly.

Gas velocities in annular gap

To determine gas velocities in the reactor pit during the blow down, two experiments were conducted at a failure pressure of 0.25 MPa and 0.5 MPa with standard geometry (L-04 and L-05, s. Table 1). However, no liquid simulant was used in these tests to avoid disturbances during the measurements due to liquid-gas interactions.

Gas velocities were measured using a Particle Image Velocimetry technique. PIV is now a well-established technique for measuring instantaneous velocity fields in flow systems [9]. Tracer particles are introduced in the flow system, and are illuminated by the very intense light of a pulsed or continuous laser. A CCD-Camera records at two consecutive known times images of the particles. The displacement of the particle images is then determined by correlating the particle image pairs of both pictures.

Figure 6 shows the experimental set up used for these investigations. Tracer particles with a size of 10 μm were introduced into the RPV by a Laskin nozzles seeding generator immediately before the start of the experiments. A pulsed Nd:YAG laser was used to illuminate the oil tracer particles. The pulse energy was approximately 20 mJ and its duration 5 ns.

($1.8 \cdot 10^{-3} \text{ m}^3$), which are 106 ms and 28 ms respectively. The blowthrough in D-22 occurs at $t = 41 \text{ ms}$, just 7 ms earlier than in D-04 (48 ms).

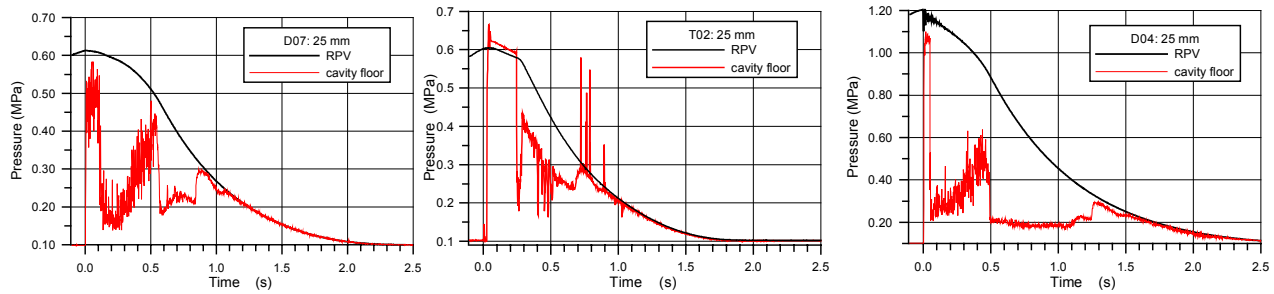


Fig. 8 Pressure histories for experiments D-07, T-02 and D-04

Dispersal fractions

The parameters used in some selected experiments as well as the obtained dispersal fractions are presented in Table 1 and Fig. 9 for comparison. The following conclusions can be obtained from these results:

- Central holes lead to large dispersal rates (Fig. 9). Depending on hole diameter and burst pressure, liquid dispersed fractions between 10 % and 75 % were obtained.

- Small lateral breaches lead to small dispersed fractions, because not all liquid is swept out of the lower head. That is to say, entrainment of liquid in the lower head cannot act below a certain liquid level and, in contrast to experiments with central holes, always some mass of liquid remains in the RPV.

- Large breaches (unzipping of lower head) lead to small dispersed fractions, because the gas can blow out of the lower head without impediment by the liquid and the blow down time is very short. There is no time for the gas to interact with the liquid and entrain it. However, small fall heights of the lower head lead to larger dispersion rates because the blow down time is longer.

- Using a larger cavity diameter (wider annular gap) the dispersion rates were only somewhat smaller.

- In the tests with the melt trapping device could be observed, that the cylinder separates the liquid at the cavity wall from the gas. The gas can flow into the compartments, while the liquid is trapped between the cylinder and the cavity wall. However, the liquid falls back into the cavity as soon as the top of the gap is reached and can be entrained by the gas, but at lower gas velocities. This reduces the dispersion substantially. For example, combining a lateral hole with the melt trapping device like in test F-06, the dispersed fraction reduces from 35.8 % (without melt trapping device) to 9.7 % (using the cylinder). Moreover, if liquid metal is employed instead of water, the dispersed fraction values could be even smaller.

- In the experiment with the 4 openings leading into the ventilation channel, no liquid was transported into the melt spreading room and just 1 % of the liquid was found in the circular channel around the cavity.

- In all experiments could be observed, that depending on the available space at the vessel support structure, a certain amount of liquid mass is caught in the space behind the conical ring, provided the liquid reaches this position.

Table 1. Dispersal fractions for different failure modes

Test	Geometry	Gas	Liquid wat/me 10^{-3} m^3	Hole Dia. (mm)	Burst Press. (MPa)	Compart. f_d	Cavity total $f_c = f_b + f_s$	RPV
D-15	central	N ₂	3.4 w	25	0.348	0.193	0.807	0
D-07	central	N ₂	3.4 w	25	0.620	0.518	0.482	0
D-04	central	N ₂	3.4 w	25	1.190	0.698	0.302	0
D-17	central	N ₂	1.8 w	25	0.612	0.407	0.593	0
H-01	central	He	3.4 w	25	0.641	0.350	0.651	0
M-02	central	N ₂	3.0 m	25	0.595	0.060	0.940	0.001
R-02	lateral s	N ₂	1.8 w	25	1.102	0.250	0.488	0.262
R-03	lateral Ø	N ₂	1.8 w	25	1.100	0.358	0.531	0.111
F-03	wider ann. gap	N ₂	3.4 w	25	1.076	0.632	0.367	0
F-04	melt trap	N ₂	3.4 w	25	1.100	0.280	0.720	0
F-06	melt trap + lateral Ø	N ₂	1.8 w	25	1.110	0.097	0.784	0.119
S-01	Vent. channel	N ₂	3.4 w	25	1.102	0.713	0.274	0
D-13	central	N ₂	3.4 w	50	0.353	0.551	0.449	0
D-06	central	N ₂	3.4 w	50	0.619	0.669	0.331	0
D-05	central	N ₂	3.4 w	50	1.200	0.759	0.241	0
T-01	stand pipe	N ₂	3.4 w	50	0.610	0.760	0.240	0
D-09	central	N ₂	3.4 w	100	1.137	0.741	0.259	0
K-03	unzip	N ₂	2.0 w	h=16	1.100	0.007	0.579	0.413
D-08	central	N ₂	3.4 w	100	0.613	0.717	0.283	0
K-01	unzip	N ₂	2.1 w	h=57	0.500	0.011	0.894	0.095
L-04	central	N ₂	0	50	0.365	-	-	-
L-05	central	N ₂	0	50	0.622	-	-	-
T-02	stand pipe	N ₂	3.4 w	25	0.604	0.553	0.447	0
D-22	central	N ₂	1.8 w	25	0.623	0.360	0.640	0
D-23	central	N ₂	1.8 w	25	1.103	0.652	0.348	0

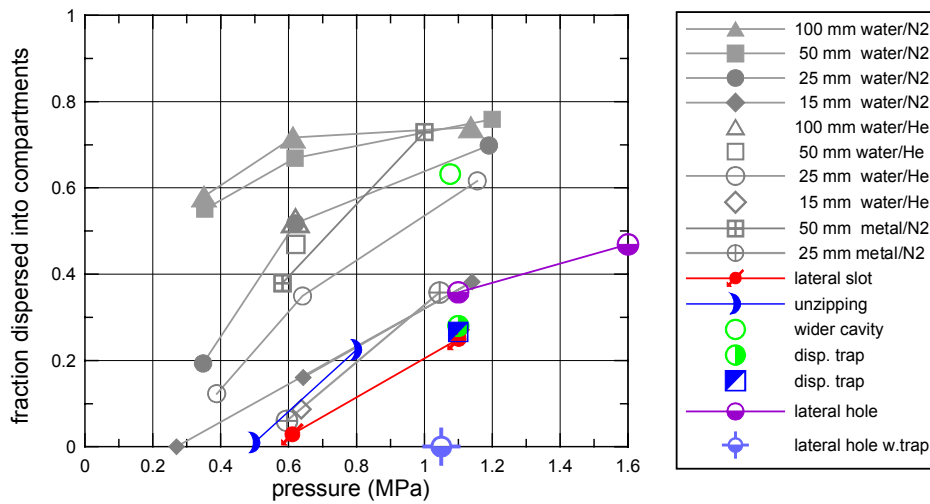


Fig. 9 Dispersed fractions for different test parameters. Experiments with central holes are represented in gray

Gas velocities in annular gap

Depending on the duration of the blow down, between 6 and 8 image pairs were taken in the experiments L-04 and L-05 with a 15 Hz frequency. From each picture pair, a 11x12 velocity vector field could be calculated. As an example, the vector field at $t = 30$ ms is presented for test L-04 in Fig. 10. Each vector represents the velocity of a 32x32 pixel cell, approximately, an area of 6x6 mm. The coordinate $x = 0$ defines the position of the RPV wall.

From experimental pressure and temperature data, a mean value for the gas velocity in the annular gap can be calculated. A comparison between this calculation and mean velocity values obtained by means of PIV is presented in Fig. 11.

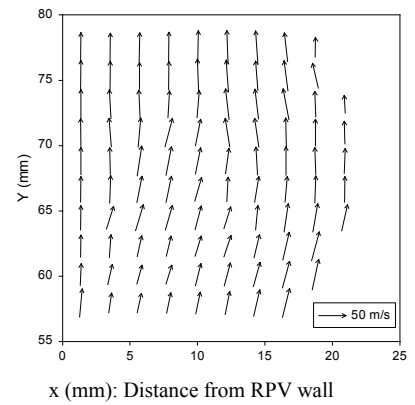


Fig.10 Vector Field in the annular gap

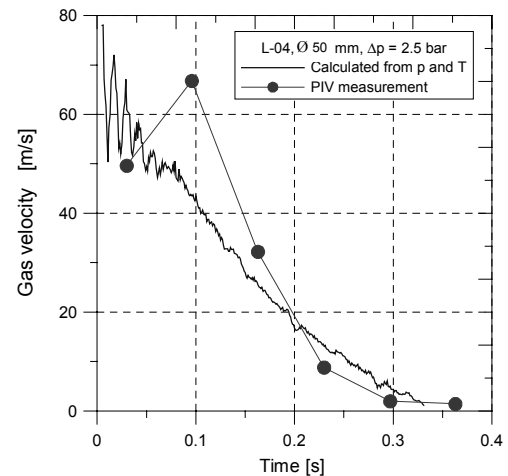
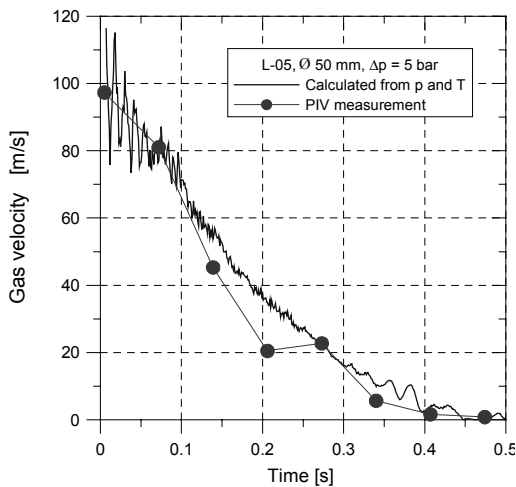


Fig. 11 PIV velocities compared with velocities calculated from experimental pressures and temperatures

From the experimental vector fields, mean velocities at constant distance from the RPV were calculated. In this way, velocity profiles at different times could be obtained as represented in Fig. 12 for both experiments.

These results show, that there is no fully developed flow at the top of the annular gap, but a flow with higher velocities close to the RPV wall. This is due to the 180° entrance effect or an effect of the blockage at the RPV support structure at the outer diameter of the annulus. This asymmetrical profile form can be observed in both experiments and disappears gradually as the blow down comes to an end, taking a flat form. Although the higher velocities could be observed closer to the RPV wall, it has to be pointed out, that also very high velocities develop close to the cavity wall. About 80 m/s could be measured in test L-05 and approximately 40 m/s in L-04, values which can lead to large liquid entrainment rates despite the short length of the annular gap.

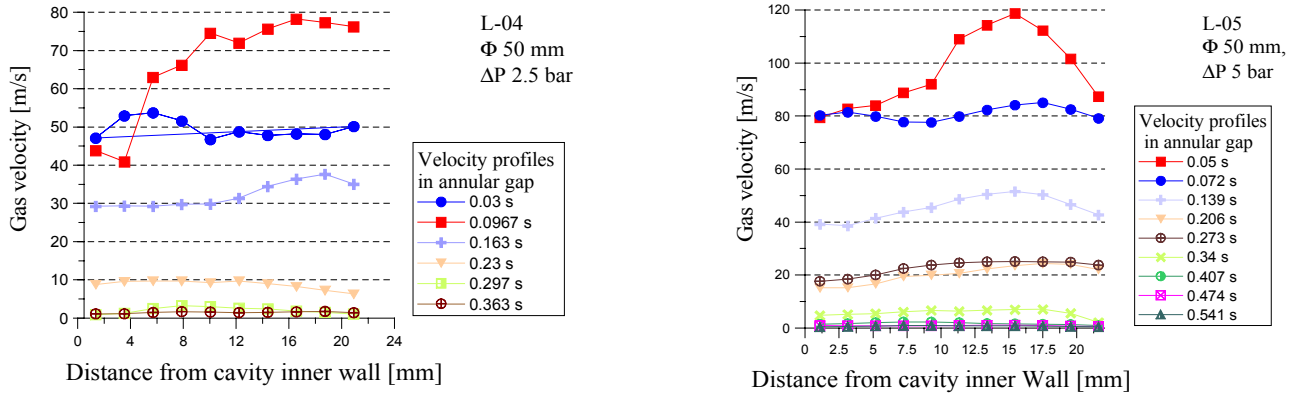


Fig. 12 Velocity profiles

Drop and liquid jet velocities

Typical velocity fields at the outlet of the main coolant lines are presented in Figs. 13a and 13b.

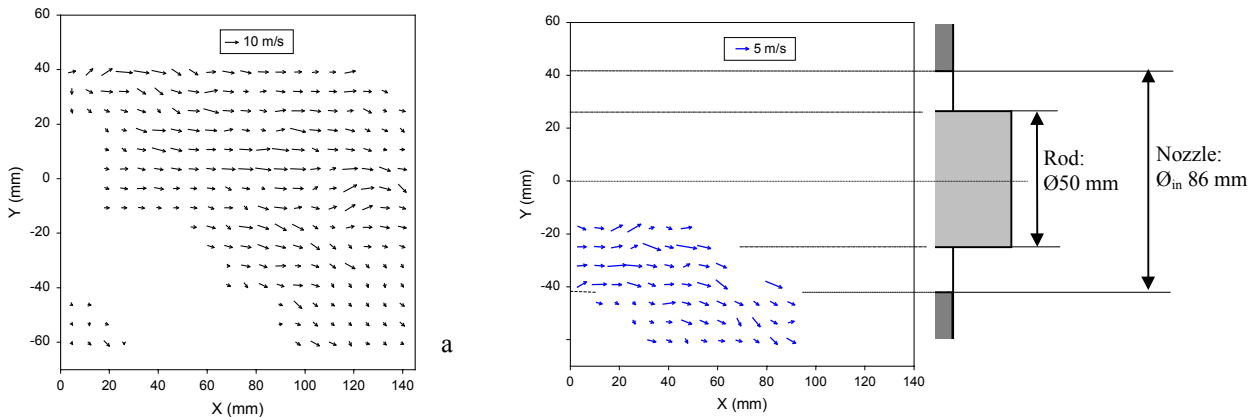


Fig. 13 Drops (a) and water jet (b) velocity fields (x = 0: end of rod; y = 0: center of rod)

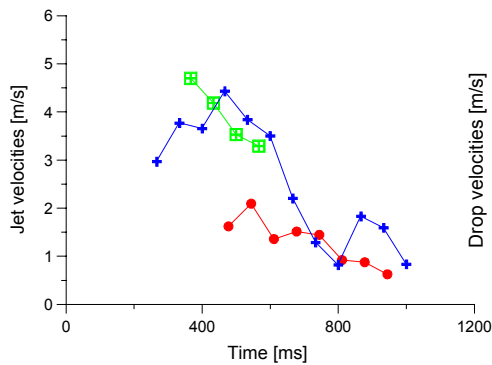


Fig. 14 Water jet velocities

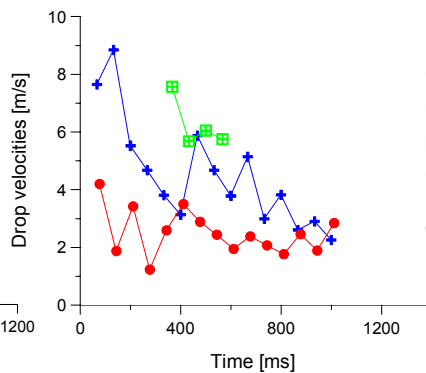


Fig. 15 Drop mean velocities

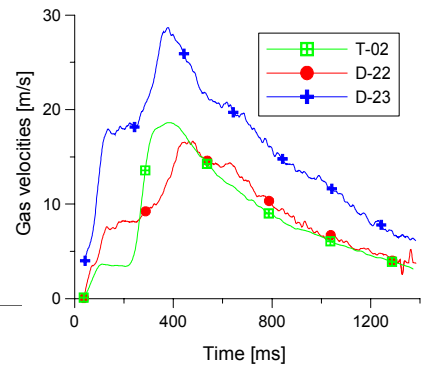


Fig. 16 Gas velocities at nozzle

In general, the droplets show large horizontal velocity components whereas the velocities in the liquid bulk show the gravity effect. Moreover, the velocities which develop in the liquid jet are lower than that calculated for droplets. To show this effect, mean velocity values were calculated for both groups and are presented versus time in Figs. 14 and 15. These results also reveal, that the different way of containing the liquid in the RPV, namely having the liquid in a pipe, leads not only to larger dispersed fractions but also to higher transport velocities out of the cavity. Concerning liquid velocities, it is almost equivalent to double the failure pressure from 0.25 MPa to 0.5 MPa as to confine the liquid in a standpipe. Relative to the droplets, even higher velocities could be observed for test T-02 at 0.5 MPa than for test D-23 at 1 MPa.

In all of the PIV measurements, a wide range of drop velocities could be observed and in many cases two velocity groups could be recognized: one low velocity group and one high velocity group. As an example, one histogram for drop velocities of one of the experiments is shown in Fig. 17. Probably, the high velocity group consists of small droplets, which are accelerated better by the gas. However, the PIV technique can just provide a mean velocity value related to the velocities of all drops contained in one cell. Therefore, no conclusions about velocities of individual drops can be drawn.

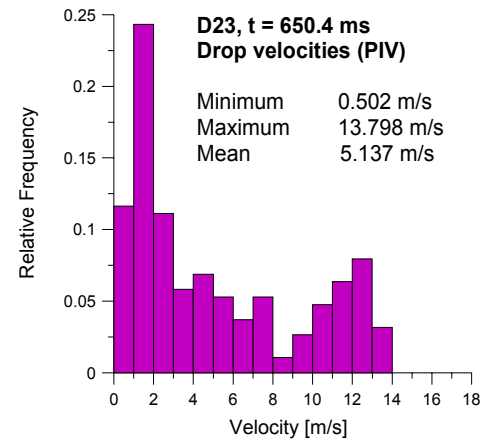


Fig. 17 Drop velocities

Drop sizes

Average drop sizes versus time are presented in Fig. 18 for the three experiments. The size range varies from 220 μm (minimum observable drop size) up to several millimeters, depending on failure pressure and test geometry. These drop size ranges are much larger than some found in the literature. This is basically due to differences in the used release modes and pressure failure ranges. In some referenced experiments, reactor cavity designs different than those presented in this work are employed [11]. In others, a similar annular cavity geometry is used but there is additionally a large flow path into the containment directly straight up [7]. Because of these differences, a comparison of all these works has to be done very carefully.

In Fig. 19 drop sizes at $t = 667$ ms for test D-22 are presented in form of a histogram.

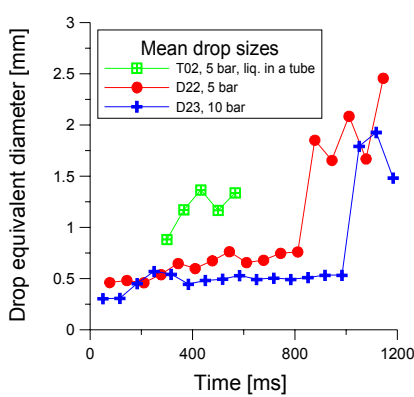


Fig. 18 Mean drop size versus time

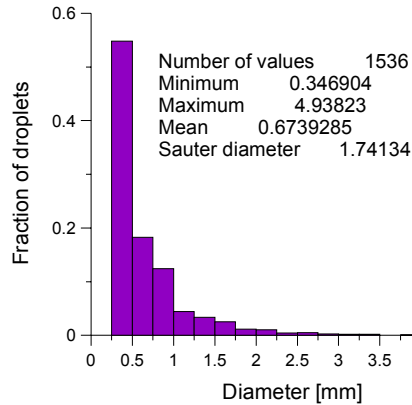
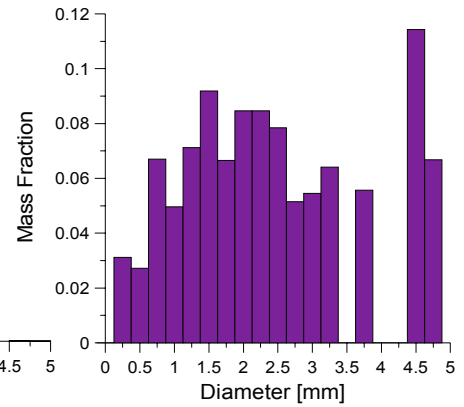


Fig. 19 Drop sizes histograms for D-22 at $t = 677$ ms



The mean drop size increases in D-23 and D-22 at the end of the dispersion process (Fig. 18) and in T-02 the same tendency can be observed.

The number of drops observed reaches a maximum at the end of the two-phase flow stage (Fig. 20). This is due to the higher gas velocities during this stage leading to higher drop fragmentation rates.

CONCLUSIONS

The DISCO-C experiments were carried out in a scaled EPR- like annular cavity design. Cold simulant materials were used to study the fluid mechanics of the dispersion process. Dispersal rates and pressure histories were analyzed employing low failure pressures and several failure modes. Moreover, measurements of drop sizes and velocities, as well as gas velocities, were presented.

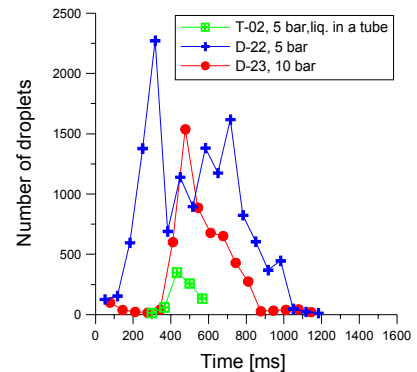


Fig. 20 Number of droplets vs. time

Concerning dispersion phenomena, the following conclusions can be drawn:

- Central hole failures lead in general to high dispersal rates. Differences could be observed depending on the hole size, burst pressure and density of the simulant materials used. The total amount of liquid is ejected out of the RPV.

- Small lateral breaches lead to less dispersion because liquid entrainment by the gas flowing out of the lower head is limited to a certain liquid level. That is to say, the liquid height in the lower head relative to the upper and lower edge of the breach plays in this case an important role. In most of these experiments some liquid remains in the RPV.

- Large lateral breaches result in low dispersion rates due to the low interaction existing between the gas and the liquid in the RPV. Here the blow down time is an additional parameter determining the dispersion process.

- A certain amount of liquid is found in the RPV support, if the liquid reaches this position.

Observing pressure histories it can be deduced, that several stages take place during the dispersion of melt: one-phase liquid flow, two-phase outflow after the blowthrough and single-phase gas flow. The time duration of all these periods depends strongly on the failure mode used.

Gas velocities in the annular gap were determined by means of PIV. The measurements show good agreement with velocities calculated from experimental pressures and temperatures. It can be concluded, that there is no fully developed flow in the annular gap. Higher velocities could be observed close to the RPV wall.

Drop sizes at the compartments range between 220 μm and several millimeters. A tendency for drop mean size to increase as gas velocities diminish could be observed. At a time close to the begin of the single-phase gas outflow, a maximal number of droplets can be observed in the experiments.

Drop velocities are larger than water jet velocities and present also larger horizontal velocity components. The gravity effect can be observed in the water jet vector fields, especially at the end of the outflow process.

From visualization of the flow phenomena at the compartments, it could be concluded, that the water jet observed in the PIV pictures is a prolongation of the liquid film observed in the reactor cavity. Therefore, drops observed in the pictures have two possible origins:

1. Drops entrained by the gas due to the shearing force exiting between gas and liquid film in the annular gap. These drops are carried out of the reactor cavity and along the main coolant lines into the compartments by the gas. They have high velocities and small diameters.
2. Drops resulting from the fragmentation of the liquid jet at the compartments. These drops have usually larger diameters and lower velocities.

The complete data of all experiments can be found in [12].

Acknowledgement: This work was partially supported by the European Commission under the contract No. FIKS-CT-1999-00003 (ECOSTAR, 5th EC-Framework Program)

REFERENCES

1. *Nucl. Eng. Des.*, Vol. 164, 1996 (Topical Issue on DCH).
2. Tutu N. K. and Gingsberg T., "Debris Dispersal from Reactor Cavities during High-Pressure Melt Ejection Accident Scenarios", *NUREG/CR 5146*, Nuclear Regulatory Commission, Washington, 1988.
3. Kim S. B., Chung M.K., Lee H.Y. and Kim M. H., "A Parametric Study of Geometric Effect on Debris Dispersal from Reactor Cavity during High Pressure Melt Ejection", *International Communications in Heat and Mass Transfer*, Vol. 22, 1995, pp.25-34.
4. Blanchat, T.K., Pilch M.M., Lee R.Y., Meyer L. and Petit M., "Direct Containment Heating Experiments at Lower Reactor Coolant System Pressure in the Surtsey Test Facility", *NUREG/CR-5746*, SAND99-1634, Sandia National Laboratories, Albuquerque, N.M., 1999.
5. Jacobs, G. and Meyer L., "Planned melt dispersal experiments in a scaled cavity", *SMiRT 14 Post-Conference Seminar on Containment of Nuclear Reactors*, CEA Saclay, France, August 25-26, 1997.
6. Wilhelm, D., "Transient Code Models for Low Pressure Corium Dispersion", *OECD Workshop on Ex-Vessel Debris Coolability*, Karlsruhe, Germany, 15-18 November 1999.
7. Bertodano, M. L. de, Becker A., Sharon A. and Schneider R., "DCH Dispersal and entrainment experiment in a scaled annular cavity", *Nucl. Eng. Des.*, Vol. 164, 1996, pp. 271-285.
8. Kim, S.B, Park R.J., Kim H.D., Chevall and Petit M., "Reactor Cavity Debris Dispersal Experiment with Simulant at Intermediate System Pressure", *Seminar Containment of Nuclear Reactors, Postconference to the 15th SmiRT*, Seoul, Korea, August 23-24, 1999.
9. "Particle Image Velocimetry", Special issue in *Measurement Science and Technology*, Vol. 8, Dec. 1997, Number 12.
10. Meyer, L., Jacobs G., Wilhelm D., Gargallo M. and Blanchat T. K., "Experiments on Corium Dispersion after Lower Head Failure at Moderate Pressure", *Seminar Containment of Nuclear Reactors, Postconference to the 15th SmiRT*, Seoul, Korea, August 23-24, 1999.
11. Wu Q., Kim S., Ishii M., Revankar S. T. and Lee R.Y., "High Pressure simulation experiment on corium dispersion in direct containment heating", *Nucl. Eng. Des.*, Vol. 164, 1996, pp. 257-269.
12. Meyer, L. Gargallo, M., Greulich, M., Kirsthaller, M., Schwall, M., Wörner, G., Wachter, E., "Low Pressure Corium Dispersion Experiments in the DISCO-C Tests Facility with Cold Simulant Fluids", *FZK-Report 6591*, Forschungszentrum Karlsruhe, to be published in 2001.